Vibrational Properties of Graphene and Nanotubes: The Radial Breathing and High Energy Modes

Presented for the Selected Topics Seminar by Pierce Munnelly
09/06/11
Supervised by Sebastian Heeg

Abstract

In the course of this review the basics of Raman spectroscopy and its use in identifying the radial breathing mode (RBM) and high energy modes (HEM) of nanotubes are discussed. Graphene is mentioned as a means of getting to the explanation of why a Raman spectrum of single-walled nanotubes appears the way it does. In analogy to the electronic band structure derivation for nanotubes mentioned in previous talks, the phonon dispersion curves of graphite will be used to arrive at a description of phonons in nanotubes. This review will concern itself with first order resonant Raman processes only, so the phonons discussed will be the Γ-point phonons of zero momentum.

Before we get to the description of how a Raman process is used, it will be useful to know the three basic steps it involves:

1. Light is incident on the sample and excites an electron to a real or virtual state
2. The electron is scattered inelastically from a phonon
3. The electron and hole recombine in a radiative transition. This is the signal that is measured in experiment.

Energy and momentum are conserved in the overall process.

Excitonic transitions are actually the dominant process in Raman spectroscopy on nanotubes. The band-to-band transitions outlined in this review are not observed because the binding energy of an exciton is much larger than k_bT at room temperature, so this bond cannot be overcome. The band-to-band picture is however sufficient to gain insight into the vibrational properties of carbon nanotubes and graphene.

Phonon Band Structure

A series of Raman spectra for graphite with successive layers of graphene removed is shown in Fig. 1; it is clear that graphite and graphene have very similar Raman spectra. The most prominent modes are the 2D and the G modes. The 2D mode involves two phonons and is described by a double-resonant Raman process. The shape of the 2D peak and the ratio of its intensity to that of the G peak is information that is crucial for determining wether graphene, few-layered graphene or graphite is present. The D-mode, a defect-induced first order double resonant process at around 1330cm^{-1}, is not shown in Fig.1. The D/G ratio is an indicator of the defect concentration and hence thequality of a given sample.
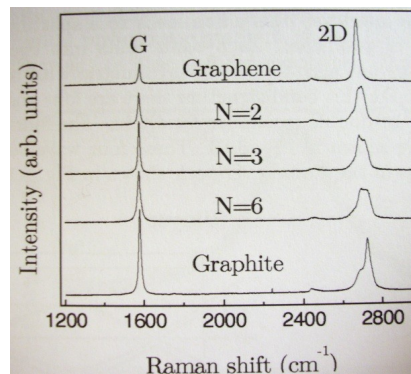

Fig. 1: Raman spectra of graphite and graphene. N indicates the number of layers of graphene. Ref. [1]

The G-mode can be visualized as in-plane out of phase oscillations of the carbon atoms involving the strong sp² bonds. This mode has zero momentum and is independent of the polarization of the incident light, as well as the arrangement of graphene planes in a graphite sample. It is however very sensitive to electron-phonon coupling, which can be varied by doping.

Fig. 2 contains a graphene phonon dispersion with three optical and three acoustic branches. Zone-folding consists of evaluating the phonon dispersion along lines of allowed circumferential wavevectors (dashed lines) of nanotubes and is a good approximation for tangential phonon dispersion at high frequencies for semiconducting tubes with diameters greater than one nanometer. Along the tube axis there are continuous allowed states. Allowed states along the circumference are represented as points separated by $2/d$ denoted with the angular momentum quantum number m,

$$\frac{-(n_{hex}-1)}{2} \leqslant m \leqslant \frac{n_{hex}}{2} \quad (1).$$

In Eq. 1, n_{hex} is equal to the number of hexagons in the nanotube unit cell, and also the number of lines in the first BZ of the nanotube. It is calculated by dividing the area of the unit cell by the area of the unit cell of graphene. That means there are $6n_{hex}$ phonon bands in the nanotube band structure. In Fig. 2, n_{hex} is 8, so m ranges from -3 to 4, and because the bands are symmetric about the gamma point all of the necessary information for this (4,4) tube is contained within this diagram. The number m indicates the number of nodes that exist for that particular mode, as shown in the inset of a); the circle is an edge-view of the tube. For larger chiral indices and chiral tubes, the number of bands can reach well into the hundreds. For example, the (14,5) tube diagram has 1104 bands. However, symmetry rules dictate that the number of Raman-active modes is much smaller, and conservation of angular momentum and the anisotropic polarizability of nanotubes further reduces the number of modes oberervable in experiment.
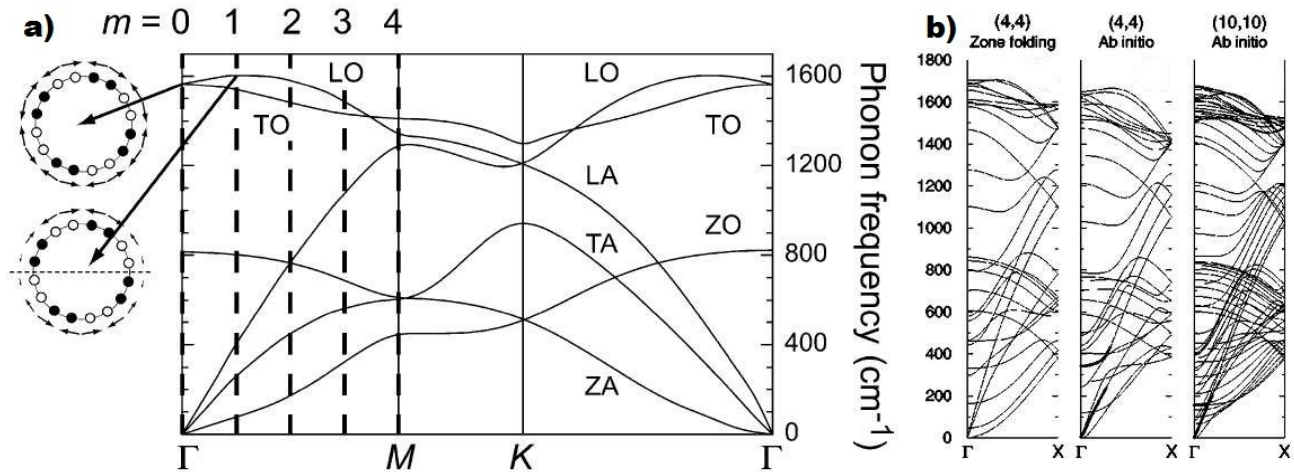

Fig. 2: a) Phonon dispersion of graphite. b) Corresponding phonon band structure for a (4,4) tube and additional (10,10) ab initio diagram illustrating how the number of phonon bands rises with chiral index. For chiral tubes, the number is even higher. Ref. [2]

Selection Rules & Antenna Effect

According to the dipole approximation, absorption or emission of a photon with polarization parallel to the tube axis does not change m for the electronic state. But with a photon whose polarization is perpendicular, the change to m can be ± 1. Thus

$\Delta m_{el} = 0, \pm 1$ (2).

Angular momentum is conserved in the Raman process. Therefore m for the phonon can be 0 if the polarizations are both parallel to the tube axis, 1 if one is parallel and the other is perpendicular, and 2 if both are perpendicular. This means

$m_{ph} = 0, 1, 2$ (3)

and that out of the 30 bands in the (4,4) tube band structure of Fig.2, only the first three are relevant.

The anisotropic polarizability of nanotubes is an effect that arises from quasi-one-dimensionality. An electric field is suppressed if it is perpendicular to the the tube axis because the charge is confined to the circumference, which is much smaller than the length of the tube itself. A field parallel to the tube builds up charge at the tube ends, very far away from each other in comparison. Fig. 3 illustrates this well as bundles of single walled nanotubes are laid out in many orientations, and depending on the direction of polarization of the laser, only Raman signals from certain segments of tubes are seen. Those tubes that lie in an orientation parallel to the polarizaion of the laser show up in as light streaks against the black background in this spatially resolved Raman spectrum. The signal used was that of the 2D peak. The fact that transitions with polarization perpendicular to the tube axis are suppressed means that m can no longer change by ± 1 as dictated by the dipole selection rules, and thus the only phonons visible in a spectrum are those with $m = 0$.
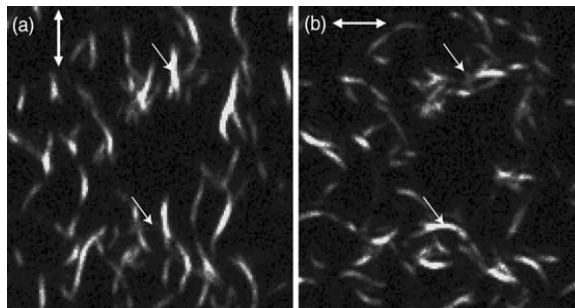

Fig. 3: Single-walled nanotubes arranged on a surface in many orientations. The double-headed arrow indicates the direction of polarization of the laser. Ref. [2]

Radial Breathing and High Energy Modes

Two very important examples of these Γ-point phonons are the radial breathing mode and the tangential high energy modes. They are important because observed together they can tell you whether you have nanotubes in a sample or not, as opposed to amorphous carbon, and because separately they allow for tube classification by chirality and family, metallic or semiconducting, as well as defect and quality measurements. Figs. 4 and 5 are representations of these modes. The arrows show the phonon eigenvectors.

At the low-energy end of a Raman spectrum, the RBM of Fig. 4 is observed, where the carbon atoms on the tube oscillate in phase radially. Its frequency ω_{RBM} is inversely proportional to the diameter of the tube. Deviations at small diameters due to curvature become significant. The RBM's typically lie between 100 and 400 cm^{-1}. Many materials have Raman spectra with peaks in this range, so the presence of nanotubes cannot be confirmed with this information alone. Also, large tube diameters give rise to close-by RBM frequencies, which makes identification difficult. Measuring the RBM frequencies of an ensemble of tubes together with the optical transition energy by resonant Raman scattering is sufficient to identify the chiral indices of the tubes.

The tangential high energy modes are in-plane out of phase oscillations of the carbon atoms, similar in origin to the G peak of graphite described at the beginning of this report, which mostly involve very strong sp^2 bonds. The frequencies are thus very high compared to the RBM. HEM's can be thought of as arising from the graphite phonon dispersion diagram with zone folding as the TO and LO branches. The tangential modes have typical wavenumbers between 1100 and 1600 cm^{-1}. For semiconducting tubes, the TO is below the LO in frequency, and for metallic tubes it is the other way around. The double peak in the spectrum at the HEM, as in Fig. 6, is a more reliable indicator of the presence of single-walled tubes than the RBM. Broadening of the HEM peak for metallic tubes will be discussed at the end of this review.
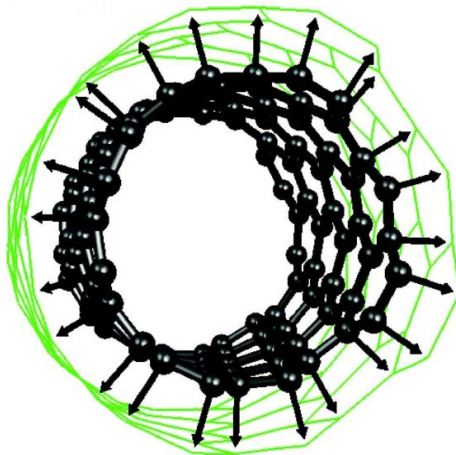

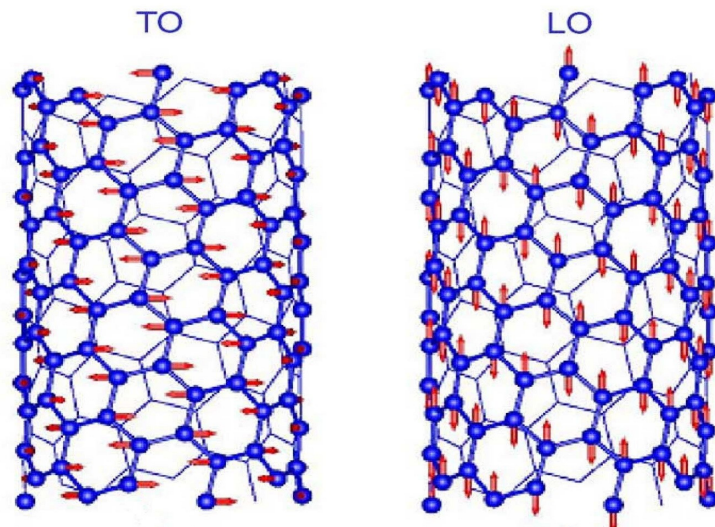Fig. 4: Radial breathing mode of an (8,4) tube. Ref. [3]

Fig. 5: Transverse and longitudinal optical high-energy modes of semiconducting tubes. Ref. [3]

Resonant Raman Spectroscopy

Resonant Raman scattering is used for the identification of RBMs and HEMs. Fig. 6 shows a typical spectrum; on the x-axis is the energy of the phonon in reciprocal centimeters. The peaks correspond to those of a single chirality.

In the experimental setup, an objective focuses the laser onto an area of about one square micron. If a sample of nanotubes is one nanometer across, the background signal would normally be expected to drown out any Raman signal of interest; however, due to resonance, the Raman signal will sharply spike in intesity and still be visible, but only if one can sufficiently block the intense Rayleigh scattered light from the detector. This is the most challenging aspect of the experiment. Fig. 7 shows how a triple grating monochromator works to that end. The first two gratings and the slits basically act together as a band-pass filter that allows the detection of Raman signals very close to the laser frequency. Grating 1 disperses the light arriving from the pinhole; intermediate slit 1 chooses a bandpass; grating 2 recombines the now dispersion-free light onto intermediate slit 2 and inside the spectrograph it is again dispersed onto the detector.

In a solution of tubes of different diameters, the RBMs will not all have the same frequency, and a series of spectra at different excitation energies must be taken. Raman resonant transitions are described by a matrix element with origins in third order perturbation theory whose square is proportional to the intensity of the Raman signal,

$$I(E_l) = \left[\frac{Mc}{\hbar \omega_{RBM}}\right]^2 \left| \frac{1}{(E_l - E_{ii} - i\gamma/2)} - \frac{1}{(E_l - \hbar \omega_{RBM} - E_{ii} - i\gamma/2)} \right|^2 \quad (4).$$

In Eq. 4, E_l is the energy of the incident laser. The intensity of the Raman signal I is proportional to the square of this matrix element. The numerator Mc consists of three terms, involving two sums over all intermediate states, the electron-phonon interaction, and the electron-radiation interaction twice, because two photons are involved. The denominator has two terms: one which gets large if the incoming photon energy matches the energy of the real excited electronic state E_{ii} and another which gets large if the outgoing photon energy (i.e. the incoming minus the phonon energy) matches it. This is why the the signal intensity becomes large if either incoming or outgoing resonance conditions are met. The lifetimes of the excited states γ are fitting parameters.
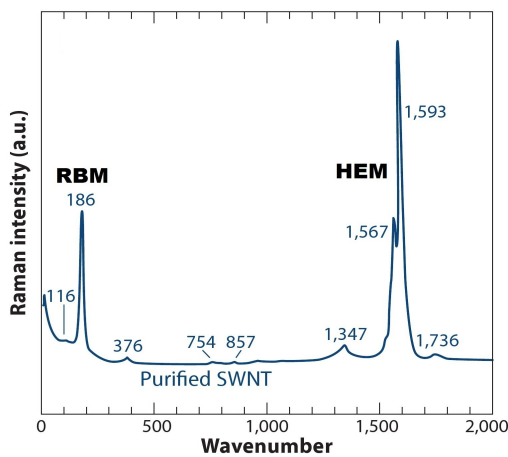

Fig. 6: Raman spectrum of single-walled nanotubes. The radial breathing and high-energy modes are labelled at the low and high energy ends, respectively. Ref. [4]
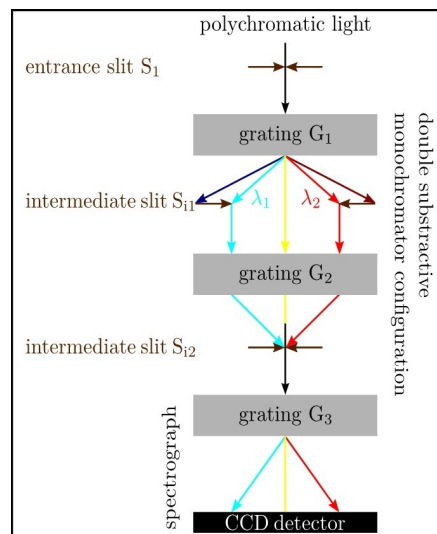

Fig. 7: Triple monochromator used to remove the Rayleigh light from the signal. Ref. [5]

Resonance occurs if the incoming or the scattered light matches the transition energy, and Fig. 8 illustrates what happens schematically. The incident or outgoing radiation is resonant if it is represented by a solid vertical line, and dashed lines indicate transitions to and from virtual states. Incoming and outgoing resonances can only be resolved if the lifetime of the electronic state is sufficiently short, and this is not the case for the RBM due to its low energy.

A resonance profile is made by taking a series of Raman spectra at different excitation energies using a tunable laser. Fig. 9 demonstrates this with an example of four RBM peaks marked with different colors. Notice that peaks gradually rise to a maximum as incoming resonance is achieved, and fall down again as outgoing resonance is left behind. As already mentioned, the incoming and outgoing resonances are so close together that they cannot be resolved separately because the energy of the RBM is so low. Each of the colored peaks arises from a tube with a different chiral index. The maximum of the resonance cross section gives the frequency (and thus the tube diameter) of the RBM.
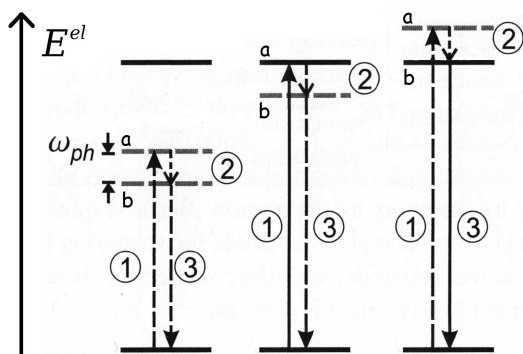

Fig. 8: One non-resonant and two resonant transitions from left to right respectively. Solid horizontal lines indicate real states, while dashed indicate virtual. Ref. [6]
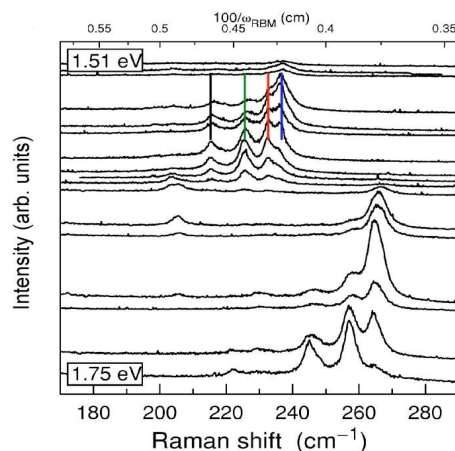

Fig. 9: Raman spectra of a sample of single-walled nanotubes at different excitation energies stacked in descending order give a resonance profile (colored lines). Ref. [7]
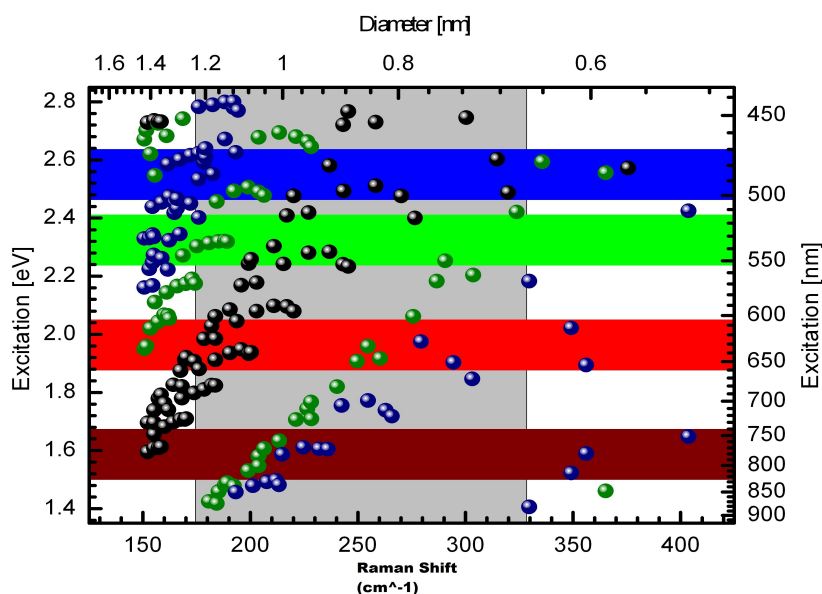

Fig. 10: Kataura plot of nanotubes. The black dots correspond to metallic tubes, while the blue and green are semiconducting. Ref. [8]
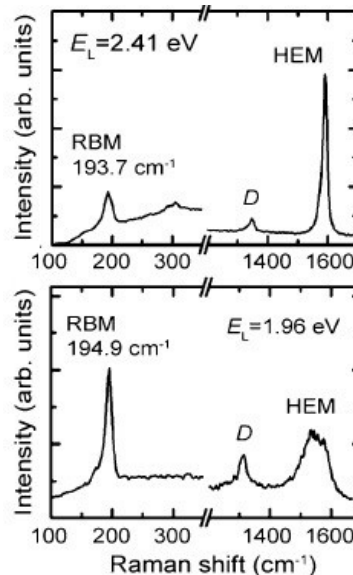

Fig. 11: Broadening of the high-energy peak in metallic tubes. Ref. [9]

Fitting the resonance profile with the Raman matrix element gives the optical transition energy. This is plotted against inverse RBM frequency, which is proportional to tube diameter, in what is known as a Kataura Plot: see Fig. 10 above for an example. In this way it is possible to compare an experimental plot with the known assignments from a Kataura plot of semiconducting tubes made by photoluminescence. It is just a matter of trigonometry to connect a tube of given diameter to its chirality,

$$d = a_0 \frac{\sqrt{n_1^2 + n_1 n_2 + n_2^2}}{\pi} \quad (5)$$

and the diameter is extracted from the RBM frequency obtained by the resonance profile. In Eq. 5, a_0 is the carbon-carbon bond length.

In closing it is worth mentioning an effect that arises from coupling between the LO phonon and low energy electronic excitations in metallic tubes. As the Fermi level is at the band crossing point, one could imagine an excitation from the valence band close by in the vicinity of the crossing point to the conduction band that has overall energy less than that of the phonon involved in scattering, and in a relaxation process photons would be emitted which do not contribute to the Raman signal. This means there is an additional decay channel open to this state which corresponds to a shortening of its lifetime, causing the peak to get broader. This can be seen in the HEM peak of the metallic tube in Fig. 11. This effect is useful for determining whether a sample contains metallic tubes or not.

Summary

This review has attempted to give an understanding of the origins and uses of two important types of phonon modes prominent in the Raman spectra of single-walled carbon nanotubes, including an outline of what a Raman process is and how it is measured. It was demonstrated how the phonon spectrum of the tubes can be extracted from that of graphite, and how the anisotropic polarizability and conservation of angular momentum lead to a restriction on the number of Raman active modes.

References

[1] courtesy of Robert Panknin

[2] C. Thomsen and S. Reich, "Raman Scattering in Carbon Nanotubes" **2007** and D. Sanchez-Portal *et al*. "Ab Initio Structural, Elastic and Vibrational Properties of Carbon Nanotubes"

[3] J. Maultzsch, H. Telg, S. Reich, and C. Thomsen. "Radial Breathing Mode of Single-walled Carbon Nanotubes: Optical Transition Energies and Chiral-index Assignment." **2005**

[4] M.S. Dresselhaus et al., "Characterizing Graphite, Graphene and Carbon Nanotubes by Raman Spectroscopy" **2010**

[5] http://www.physik.fu-berlin.de/en/einrichtungen/ag/ag-reich/ausstattung/raman/index.html

[6] adapted from S. Reich, C. Thomsen, J. Maultzsch; "Carbon Nanotubes: Basic Concepts and Physical Properties"

[7] J. Maultzsch, H. Telg, S. Reich, and C. Thomsen. "Radial Breathing Mode of Single-walled Carbon Nanotubes: Optical Transition Energies and Chiral-index Assignment." **2005**

[8] courtesy of Sebastian Heeg

[9] from C. Thomsen and S. Reich, "Raman Scattering in Carbon Nanotubes" (2007)

The Master thesis of Benjamin Hatting was helpful in the preparation of this presentation.